Astron. Astrophys. 319, 290–304 (1997)

ASTRONOMY
AND
ASTROPHYSICS

Resonance and chaos

I. First-order interior resonances

O.C. Winter[1,2] **and C.D. Murray**[2]

[1] Grupo de Dinâmica Orbital e Planetologia, Campus Guaratinguetá, UNESP, CP 205, CEP 12500-000, Guaratinguetá, São Paulo, Brazil
[2] Astronomy Unit, Queen Mary and Westfield College, University of London, Mile End Road, London E1 4NS, UK

Received 15 May 1996 / Accepted 22 July 1996

Abstract. Analytical models for studying the dynamical behaviour of objects near interior, mean motion resonances are reviewed in the context of the planar, circular, restricted three-body problem. The predicted widths of the resonances are compared with the results of numerical integrations using Poincaré surfaces of section with a mass ratio of 10^{-3} (similar to the Jupiter–Sun case). It is shown that for very low eccentricities the phase space between the 2:1 and 3:2 resonances is predominantly regular, contrary to simple theoretical predictions based on overlapping resonance. A numerical study of the 'evolution' of the stable equilibrium point of the 3:2 resonance as a function of the Jacobi constant shows how apocentric libration at the 2:1 resonance arises; there is evidence of a similar mechanism being responsible for the centre of the 4:3 resonance evolving towards 3:2 apocentric libration. This effect is due to perturbations from other resonances and demonstrates that resonances cannot be considered in isolation. On theoretical grounds the maximum libration width of first-order resonances should increase as the orbit of the perturbing secondary is approached. However, in reality the width decreases due to the chaotic effect of nearby resonances.

Key words: chaos – celestial mechanics – minor planets

1. Introduction

The well-documented preference for commensurability between the orbital periods of solar system objects (Roy & Ovenden 1954) shows the importance of resonant phenomena in the dynamical evolution of the solar system. The existence of a mean motion resonance between a pair of objects can lead to a repeating geometrical configuration of the orbits which guarantees stability. Even if the resonance is not exact, there is still the possibility of stable librational motion around an equilibrium point. Therefore it is important to have an understanding of the dynamics of resonance and to develop analytical models which accurately reflect the true nature of resonant interactions.

In this paper we consider the dynamics of resonance in the context of the planar, circular, restricted three-body problem. This is, perhaps, the simplest dynamically meaningful problem that exhibits the various phenomena associated with resonance, including regular and chaotic motion. In the current paper we are particularly interested in the motion of the test particle in the vicinity of the major first-order interior resonances. One of the greatest advantages of the circular restricted problem is that the existence of an integral of the motion (the Jacobi constant) allows us to study such behaviour by means of a Poincaré surface of section. The circular problem also has the advantage of simplifying the various analytical models.

The main aim of this paper is to review, clarify and test the various analytical models that have been used in the study of interior first-order resonances. The validity of each model is tested against the results of numerical integrations of the full equations of motion. One analytic attempt to study resonant motion uses the pendulum approximation (see Dermott & Murray 1983). This is the 'ideal resonance problem' and it is based on the assumption that the particle is sufficiently close to the resonant location given by the exact commensurability of the mean motions. We show that this assumption requires that the orbital eccentricity of the particle is sufficiently large. The study of resonances for small eccentricities usually follows another model based on Andoyer's Hamiltonian, also called the 'second fundamental model of resonance' (Andoyer 1903, Henrard & Lemaître 1983). In this model the particle does not necessarily have to be close to the nominal resonant position; the only restriction is that the eccentricity has to be small. Therefore, the problem can be divided into two classes depending on the eccentricity of the particle's orbit. We are particularly interested in the effects of small eccentricity on the location and size of the resonant libration regions, and the stability of nearly circular orbits. We follow the evolution of the libration regions associated with the 2:1, 3:2 and 4:3 interior resonances, comparing the results of full numerical integration with those predicted from the analytical models.

The current paper represents one part of Project CRISS-CROSS (Chaotic Regions of the Inner Solar System – Chaotic

Regions of the Outer Solar System). The ultimate goal of this project is to understand the location and origin of chaotic regions of the phase space of the solar system. We have already carried out extensive numerical integrations of the planar, circular, restricted three-body problem and mapped out a large part of the phase space interior to the orbit of the secondary mass (Winter & Murray 1994a). A similar study for exterior motion has also been carried out (Winter & Murray 1994b). In each case we used a secondary/primary mass ratio of 10^{-3}, similar to that of the Sun–Jupiter system. We have already discussed some of the preliminary results of this work relating to the surface of section method and the Liapunov characteristic exponent (Winter & Murray 1995, 1996a). In the current study we make use of the numerical results from Winter & Murray (1994a,b) in order to compare the different analytical approaches to interior, first-order resonance. A companion paper (Winter & Murray 1996b) examines the case of first-order, exterior resonances; future papers will discuss other phenomena.

In Sect. 2 we describe the planar, circular restricted three-body problem and present an analysis of the variation of the orbital elements of the test particle near a resonance. This approach leads to a discussion of the pendulum model (Sect. 3) and its predictions of resonance width. A Hamiltonian approach to the resonance problem is presented in Sect. 4 and the problem is considered for large and small values of the particle's eccentricity. The results of the numerical integrations and the comparison with theory are given in Sect. 5. In Sect. 6 we present the results of a series of numerical integrations at the 2:1 interior resonance. These illustrate the various phenomena discussed elsewhere in the paper. A summary of our conclusions is presented in Sect. 7.

2. Variation of the orbital elements

The planar, circular restricted three-body problem consists of two bodies — a primary or central body (of mass m_1), a secondary or perturbing body (of mass m_2), both moving in circular orbits about their common centre of mass, and a test particle moving under the gravitational effect of the other two masses without affecting their motion.

If the particle has position vector (x, y) and velocity vector $(\dot{x}, \dot{y})$ then the equations of motion in a uniformly rotating frame with the x-axis lying along the primary–secondary line are given by

$$\ddot{x} - 2\dot{y} - x = -\bar{m}_1 \frac{x + \bar{m}_2}{r_1^3} - \bar{m}_2 \frac{x - \bar{m}_1}{r_2^3} \tag{1}$$

$$\ddot{y} + 2\dot{x} - y = -\left(\frac{\bar{m}_1}{r_1^3} + \frac{\bar{m}_2}{r_2^3} \right) y \tag{2}$$

where the constants $\bar{m}_1$ and $\bar{m}_2$ are the reduced masses given by $\bar{m}_1 = m_1/(m_1 + m_2)$ and $\bar{m}_2 = m_2/(m_1 + m_2)$, and the squares of the distances of the test particle from the centre of mass and the two masses are given by $r^2 = x^2 + y^2$, $r_1^2 = (x + \bar{m}_2)^2 + y^2$ and $r_2^2 = (x - \bar{m}_1)^2 + y^2$, respectively. In this system of units $\bar{m}_1 + \bar{m}_2 = 1$ and the origin is at the centre of mass of the system. The constant separation of the two masses is taken to be the unit of distance and the angular velocity of the rotating frame is taken to be unity; this is also the mean motion of either mass about the centre of mass. Consequently the orbital period of the secondary is 2π time units.

In the restricted problem neither the orbital energy nor the angular momentum are conserved since the test particle does not affect the motion of the other two bodies. However, the dynamical system still has an integral of the motion, the Jacobi constant, given by

$$C_\mathrm{J} = x^2 + y^2 + 2\left(\frac{\bar{m}_1}{r_1} + \frac{\bar{m}_2}{r_2} \right) - \dot{x}^2 - \dot{y}^2. \tag{3}$$

The structure of the phase space of this dynamical system is mainly determined by resonant phenomena. In such situations there is a commensurability between the mean motion of the particle, n, and the mean motion of the secondary mass (the perturber), n', such that $(p + q)n' \approx pn$, where p and q are integers. In this case the particle and the perturbing mass are said to be close to the $p+q : p$ mean motion resonance and q is called order of the resonance. In this paper we are concerned with the $q = 1$ (first-order) resonances interior to the perturber (i.e. $n > n'$). We can study the orbital evolution of the test particle by direct numerical integration of the equations of motion given above, making use of the Jacobi constant to generate Poincaré surfaces of section.

An analytical understanding of the evolution can be achieved by considering the variation of the orbital elements. In the remainder of this section we carry out a simple analysis of the variation of the orbital elements using Lagrange's planetary equations. The equations for the time variation of the semimajor axis, a, the mean motion, n, the eccentricity, e, the longitude of pericentre, ϖ, and the mean longitude at epoch, ϵ are given by

$$\dot{a} = \frac{2}{na} \frac{\partial \mathscr{R}}{\partial \lambda} \tag{4}$$

$$\dot{n} = -\frac{3}{a^2} \frac{\partial \mathscr{R}}{\partial \lambda} \tag{5}$$

$$\dot{e} = -\frac{\sqrt{1 - e^2}}{na^2 e} \left(1 - \sqrt{1 - e^2} \right) \frac{\partial \mathscr{R}}{\partial \lambda} - \frac{\sqrt{1 - e^2}}{na^2 e} \frac{\partial \mathscr{R}}{\partial \varpi} \tag{6}$$

$$\dot{\varpi} = \frac{\sqrt{1 - e^2}}{na^2 e} \frac{\partial \mathscr{R}}{\partial e} \tag{7}$$

$$\dot{\epsilon} = -\frac{2}{na} \frac{\partial \mathscr{R}}{\partial a} + \frac{\sqrt{1 - e^2}}{na^2 e} \left(1 - \sqrt{1 - e^2} \right) \frac{\partial \mathscr{R}}{\partial e} \tag{8}$$

(see, e.g., Brouwer & Clemence 1961) where $\lambda = \int n \, \mathrm{d}t + \epsilon$ is the mean longitude and $\mathscr{R}$ is the perturbing potential experienced by the particle due to the mass m_2. In keeping with our notation for orbital elements, primed quantities refer to the perturber and unprimed quantities refer to the particle. Hence $m' = m_2$ is the mass of the perturber and we define $M = m_1$ to be the mass of the central object.

It can be shown that the term associated with the resonant angle $\varphi = j_1\lambda' + j_2\lambda + j_3\varpi$ (where j_1, j_2 and j_3 are integers) is given by

$$\mathscr{R} = (-1)^{j_3} \frac{\mathscr{G}m'}{a'} f(\alpha) e^{|j_3|} \cos\varphi \tag{9}$$

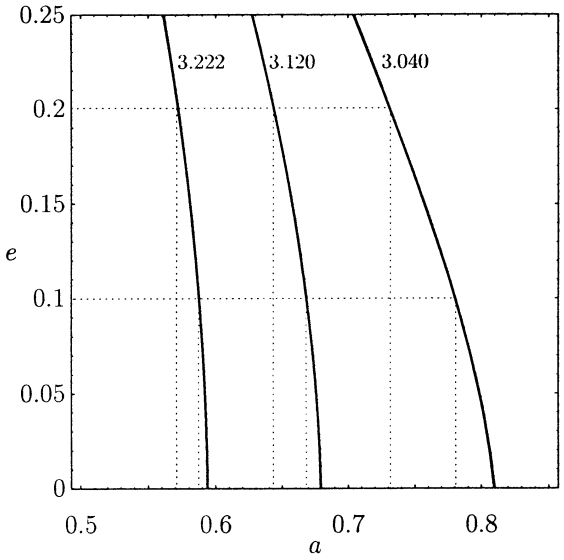

Fig. 1. Curves of constant Jacobi constant in a–e space for a particle at pericentre at inferior conjunction The values of the Jacobi constants are 3.040, 3.120 and 3.222. Note that for a fixed value of Δe, the corresponding value of Δa decreases as e decreases.

where $\mathscr{G}$ is the universal gravitational constant, $f(\alpha)$ is a function of $\alpha = a/a'$ and we have included only the lowest order term in e (Dermott & Murray 1983).

If the resonant term in the disturbing function is considered to dominate and we neglect all other terms, we can substitute the partial derivatives of $\mathscr{R}$ in Lagrange's equations to obtain

$$\dot{a} = -2j_2 \mathscr{C} a e^{|j_3|} \sin\varphi \tag{10}$$

$$\dot{n} = 3j_2 \mathscr{C} n e^{|j_3|} \sin\varphi \tag{11}$$

$$\dot{e} = \mathscr{C} e^{|j_3|-1} \sqrt{1-e^2} \left\{ j_3 + j_1 \left(1 - \sqrt{1-e^2}\right) \right\} \sin\varphi \tag{12}$$

$$\dot{\varpi} = |j_3|\, \mathscr{C} e^{|j_3|-2} \sqrt{1-e^2} \cos\varphi \tag{13}$$

$$\dot{\epsilon} = |j_3|\, \mathscr{C} e^{|j_3|-2} \sqrt{1-e^2} \left(1 - \sqrt{1-e^2}\right) \cos\varphi \tag{14}$$

where, using Kepler's third law,

$$\mathscr{C} = (-1)^{j_3} (m'/M) n \alpha f(\alpha). \tag{15}$$

Note that for these purposes we have assumed a to be a constant such that there is no contribution from the first term in the equation for $\dot{\epsilon}$.

D'Alembert's rule requires that the sum of the coefficients of angles of longitude in φ must be zero. A resonance of the form $(p+q)n' \approx pn$ can be studied by selecting a resonant angle φ with $j_1 = (p+q)$, $j_2 = -p$ and $j_3 = -q$. Thus $|j_3|$ is the order of the resonance. Hence, from Eqs. (10–14), it can be seen that for resonances of order 2 or greater, all terms involving negative powers of the eccentricities disappear. Therefore the effects of low eccentricity are only important for first-order resonances.

In the case of interior, first-order resonances the resonant angle has the form $\varphi = j\lambda' + (1-j)\lambda - \varpi$ (i.e. $j_1 = j, j_2 = 1-j$, $j_3 = -1$) and it can be shown that

$$f(\alpha) = j b_{1/2}^{(j)} + \frac{\alpha}{2} \frac{\mathrm{d} b_{1/2}^{(j)}}{\mathrm{d}\alpha} \tag{16}$$

(Murray & Harper 1993) where $b_{1/2}^{(j)}$ is a Laplace coefficient which can be calculated numerically by evaluating a hypergeometric function (as a series in α) or by using

$$b_{1/2}^{(j)}(\alpha) = \frac{1}{\pi} \int_0^{2\pi} \frac{\cos j\theta \, \mathrm{d}\theta}{(1 - 2\alpha\cos\theta + \alpha^2)^{1/2}}. \tag{17}$$

In our case, $j = 2$ corresponds to the 2:1 resonance, $j = 3$ to the 3:2 resonance, etc.

Including terms up to first order in e, Lagrange's equations for motion near a first-order resonance become

$$\dot{a} = -2(1-j) \mathscr{C} a e \sin\varphi \tag{18}$$

$$\dot{n} = 3(1-j) \mathscr{C} n e \sin\varphi \tag{19}$$

$$\dot{e} = -\mathscr{C} \sin\varphi \tag{20}$$

$$\dot{\varpi} = \mathscr{C} \frac{1}{e} \cos\varphi \tag{21}$$

$$\dot{\epsilon} = \mathscr{C} \frac{e}{2} \cos\varphi \tag{22}$$

From the above equations we can deduce some of the properties of motion near first-order resonances for the special case of small eccentricities:

- a is almost constant since $\dot{a}$ is linearly dependent on e; consequently $\mathscr{C}$ is also nearly constant, justifying our previous assumption.
- $\dot{e}$ is independent of e, so it is a factor $\sim 1/e$ larger than $\dot{a}$.
- $\dot{\varpi}$ is large for near circular orbits.
- $\dot{\epsilon}$ is small, implying that ϵ is almost constant for near circular orbits.
- $\dot{a}$ and $\dot{e}$ have opposite signs; therefore, when a is increasing e is decreasing and vice-versa.

The rate of variation of the orbital elements given in Eqs. (18–22) involves the sine or cosine of the resonant angle, φ. The coefficients of these functions give the maximum variation for each orbital element. For small eccentricities the maximum variation of e is almost constant while the maximum variation of a decreases as e decreases. This analysis can also be visualised with the help of contour plots of the Jacobi constant in the a–e plane for a fixed value for ϖ. Fig. 1 shows such plots for a particle at pericentre at inferior conjunction covering the range of semimajor axis and eccentricity of interest. Note that since the unit of distance is defined by $a' = 1$, a and $\alpha = a/a'$ are identically equal.

In Fig. 1 the particle was chosen to be at pericentre at inferior conjunction because this is the configuration that is expected to give rise to the largest change in a and e. Although ϖ changes rapidly at low e, it can be shown that the curve in the a–e space does not change significantly for different values of ϖ. Therefore, it is reasonable to assume that the changes in a and e will have to be such that the (a, e) point remains on the curve defined by the relevant Jacobi constant for a fixed ϖ. From Fig. 1 we can see that for equally spaced intervals of the eccentricity, Δe, the corresponding intervals of semimajor axis, Δa vary such

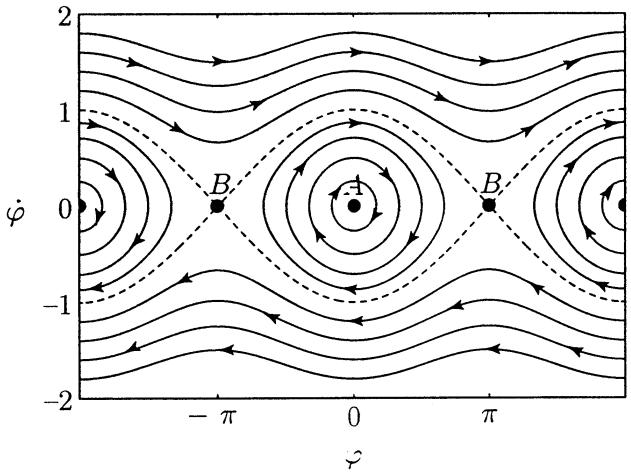

Fig. 2. Phase space of a pendulum-like system. The separatrix (dashed line) passing through the unstable point B is the boundary between the librational motion (closed curves) about the stable point A and the region of circulation (continuous curves).

that as e decreases Δa also decreases and a can reasonably be assumed constant at very low values of e.

An exact resonance exists where the time derivative of a particular resonant argument is identically equal to zero. For a general argument this occurs where

$$\dot{\varphi} = j_1 n' + j_2(n + \dot{\epsilon}) + j_3 \dot{\varpi} = 0 \tag{23}$$

and at this location the resonant angle φ is stationary. If the $\dot{\epsilon}$ and $\dot{\varpi}$ in Eq. (23) are neglected, resonance occurs at the exact commensurability of the mean motions with $j_1 n' + j_2 n = 0$, where j_1 and j_2 have opposite sign. We refer to this as the *nominal* location of the resonance. Therefore, from Kepler's third law, the semimajor axis of the nominal resonance is given by

$$a_{\rm nom} = (-j_2/j_1)^{2/3} a'. \tag{24}$$

We have seen that for first-order resonances with small eccentricity $\dot{\epsilon}$ is small and can still be neglected. However, $\dot{\varpi}$ is large and has to be included in the determination of the location of the exact resonance. In this case the resonant semimajor axis is shifted from the nominal position due to the $\dot{\varpi}$ contribution in Eq. (23). The sign of $\dot{\varpi}$ determines whether the resonant semimajor axis is larger or smaller than the nominal one. For interior, first-order resonances $f(\alpha) > 0$ and $\mathscr{C} < 0$. Hence $\dot{\varpi} < 0$ for $\varphi = 0$ and the resonant semimajor axis is smaller than the nominal value. Conversely, $\dot{\varpi} > 0$ for $\varphi = \pi$, and the resonant semimajor axis is larger than the nominal value.

The equation of motion of the first-order resonant argument φ is obtained by taking its second time derivative:

$$\ddot{\varphi} = j_2 \dot{n} + j_2 \ddot{\epsilon} + j_3 \ddot{\varpi} \tag{25}$$

where, for a general resonance,

$$\ddot{\epsilon} = j_3 \mathscr{C} \left(\frac{\partial F(e)}{\partial e} \dot{e} \cos\varphi - F(e) \dot{\varphi} \sin\varphi \right) \tag{26}$$

$$\ddot{\varpi} = j_3 \mathscr{C} \left(\frac{\partial G(e)}{\partial e} \dot{e} \cos\varphi - G(e) \dot{\varphi} \sin\varphi \right) \tag{27}$$

with

$$F(e) = e^{|j_3|-2} \sqrt{1-e^2} \left(1 - \sqrt{1-e^2} \right) \tag{28}$$

$$G(e) = e^{|j_3|-2} \sqrt{1-e^2}\,. \tag{29}$$

Note that the contribution due to $\ddot{\epsilon}$ and $\ddot{\varpi}$ can be neglected in almost all cases since they are a factor m'/M smaller than $\dot{n}$ ($m'/M \approx 10^{-3}$ for the Jupiter-Sun system). Note that the second term on the right-hand side of the $\ddot{\epsilon}$ and $\ddot{\varpi}$ equations (Eq. (26,27)) have the same powers of m'/M as $\dot{n}$ but they are multiplied by $\dot{\varphi}$ which is small near the resonant position. However, for first-order resonances with small e, $\ddot{\varpi}$ is inversely proportional to e, and the $\ddot{\varpi}$ cannot be neglected. In order to find all the possible values of a and e for which a resonant argument is librating and therefore in resonance, Dermott & Murray (1983) considered the cases of small and large e using the pendulum approximation. In the next section we follow their work and apply the resulting model to the 2:1, 3:2 and 4:3 resonances.

3. Pendulum model

For first-order resonances with large eccentricity ($e \geq 0.15$) and for any higher order resonance, Eq. (25) can be well approximated by including just the lowest order terms in the m'/M, giving

$$\ddot{\varphi} = 3 j_2^2 n e^{|j_3|} \mathscr{C} \sin\varphi\,. \tag{30}$$

This corresponds to a simple pendulum equation (cf. $\ddot{\varphi} = -w_0^2 \sin\varphi$) when n, e and $\mathscr{C}$ are assumed to be constant. The various types of motion of φ can be visualized from the well known topology of the phase space of the pendulum (see Fig. 2). The phase space has two equilibrium points, one (A) is stable, and the other (B) is unstable. The types of motion can be classified as either libration or circulation. The division is made by the trajectory that passes through the unstable equilibrium point (dashed line in Fig. 2); this is the *separatrix*. Trajectories within the separatrix exhibit *libration*. In such trajectories the resonant angle φ oscillates ($\dot{\varphi}$ changes sign periodically), and the amplitude of oscillation is less than 2π. For the trajectories outside the separatrix φ exhibits *circulation*. In this case the variation of $\dot{\varphi}$ has a fixed sign such that φ is always increasing ($\dot{\varphi} > 0$) or decreasing ($\dot{\varphi} < 0$).

The maximum libration of φ determined by the separatrix gives the boundaries of all the values of a and e for which the trajectory is said to be in resonance. By finding the energy integral for the separatrix, given by the energy at the unstable equilibrium point, and comparing it with the time derivative of φ one can find the maximum deviation of mean motion from the nominal value $n_{\rm nom}$, given by the exact commensurability of the mean motions ($n_{\rm nom} = (-j_1/j_2)n'$). From Dermott & Murray (1983) this is

$$\delta n = \pm \sqrt{12 n |\mathscr{C}| e^{|j_3|}} = \pm \sqrt{\frac{12 \mathscr{G} m' |f(\alpha)| e^{|j_3|}}{a' a^2}}\,. \tag{31}$$

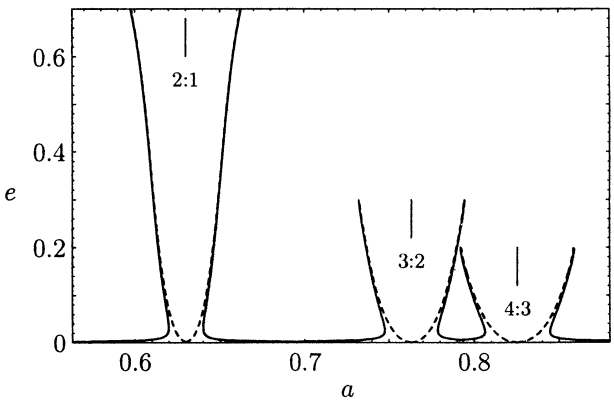

Fig. 3. Maximum libration regions in (a, e) space derived using the pendulum approach for the 2:1, 3:2 and 4:3 resonances. The dashed line is the libration width derived by neglecting the pericentre contribution; the solid line includes the pericentre contribution. The locations of the nominal resonant semimajor axes are indicated at the top of the diagram.

For first-order resonances with low e the $\ddot{\varpi}$ contribution becomes important; from Eq. (27) it can be approximated by

$$\ddot{\varpi} = \frac{\mathscr{C}^2}{2e^2}\sin 2\varphi - \frac{\mathscr{C}}{e}(jn' + (1-j)n)\sin\varphi \,. \tag{32}$$

Hence Eq. (25) becomes

$$\begin{aligned}\ddot{\varphi} = &\left\{3(1-j)^2 en\mathscr{C} + \frac{\mathscr{C}}{e}(jn' - (1-j)n)\right\}\sin\varphi \\ &- \frac{\mathscr{C}^2}{2e^2}\sin 2\varphi \,.\end{aligned} \tag{33}$$

This equation can be considered as a modified pendulum equation. By finding the energy integral of the separatrix (given by the energy at the unstable equilibrium point) and making use of $\dot{\varphi}$, the maximum change in n is found to be (Dermott & Murray 1983)

$$\begin{aligned}\delta n &= -\frac{|\mathscr{C}|}{3(1-j)e} \pm \sqrt{12|\mathscr{C}|ne\left(1 + \frac{|\mathscr{C}|}{27(1-j)^2e^3n}\right)} \\ &= -\frac{(m'/M)n\alpha|f(\alpha)|}{3(1-j)e} \pm \left[12(m'/M)n^2\alpha|f(\alpha)|e\right]^{1/2} \\ &\quad \times \left[1 + \frac{(m'/M)\alpha|f(\alpha)|}{27(1-j)^2e^3}\right]^{1/2} \,.\end{aligned} \tag{34}$$

The first term on the right-hand side of Eq. (34) represents a shift in the location of the exact resonance; this must occur when the average of $\dot{\varpi}$ is non-zero. The second term is the maximum variation in n that can occur, including the effect of a low eccentricity pericentre variation. From Kepler's third law the corresponding variation in semimajor axis, δa, is given by

$$\delta a = -\frac{2a}{3n}\delta n \,. \tag{35}$$

Therefore, for a given first-order resonance and eccentricity the maximum libration in semimajor axis can be found from Eq. (35) and Eq. (31) (if the pericentre variation can be neglected) or Eq. (34) (if e is small and there is a pericentre contribution). We have computed these variations for the 2:1, 3:2 and 4:3 resonances, and the results are shown in Fig. 3. For each resonance a different maximum value of eccentricity was considered during the computations due to the problem of convergence of the disturbing function for larger values of e. The dashed lines in Fig. 3 show the parabolic shape resulting from neglecting the effects due to small e (i.e. using Eq. (31)). Note that with this approach there is no overlap of the libration regions for low e. This is not the case when Eq. (34) is used (the solid lines in Fig. 3). For small eccentricity ($e \leq 0.02$) the plot appears to imply that any value of a would place the particle in the libration region of all three resonances and consequently there would be overlap in the (a, e) plane for all these first-order resonances. The overlap of resonances is generally used as a criterion for the onset of chaotic motion (Chirikov 1979). In the overlap region the particle would have to be librating simultaneously in two different resonances leading to chaotic behaviour. Note that the difference between the two approaches shown in Fig. 3 only occurs for eccentricities smaller than 0.1. In fact, as we show below, the region of low e is *not* associated with simultaneous libration in several resonances.

4. Hamiltonian approach

Another common approach to the resonance problem is to use a Hamiltonian treatment. This has the advantage of using canonical variables and making transformations that can simplify the underlying dynamics of the problem. On the other hand, successive transformations can make it difficult to visualise the effect of the resonance on the orbital elements. In terms of the Delaunay canonical elements (see, e.g., Brouwer & Clemence 1961) the Hamiltonian for the planar, circular, restricted three-body problem is given by

$$\mathscr{H} = -\frac{\mu_1^2}{2L^2} - \mathscr{R} \tag{36}$$

where $\mu_1 = \mathscr{G}M$, and $L = \sqrt{\mu_1 a}$ is the momentum canonical to the mean anomaly, l. The first term on the right-hand side of the equation corresponds to the two-body Hamiltonian and the second term is the complete disturbing function due to the perturber. $\mathscr{R}$ can be written as

$$\mathscr{R} = \mu_2 \sum_{i=0}^{\infty}\sum_{j=-\infty}^{\infty} K^{(i,j)}\cos(il + j(t-g)) \tag{37}$$

where $\mu_2 = \mathscr{G}m'$, g is the longitude of periapse (in the planar problem) and is conjugate to the momentum, $G = L\sqrt{1-e^2}$, and $K^{(i,j)}$ is a function of L and G.

A resonance occurs when one of the cosine arguments in the disturbing function is nearly stationary. This means that there is a commensurability of frequencies of the system. Since the Hamiltonian is time dependent, the equation for the resonance condition has the form

$$(p+q)\dot{l}(L,G) - p\{1 - \dot{g}(L,G)\} = 0 \tag{38}$$

where p and q are integers and the frequencies $\dot{l}$ and $\dot{g}$ are given by Hamilton's equations neglecting all the periodic terms of the Hamiltonian (Eq. (36)). Hence

$$\dot{l} \equiv \frac{\partial}{\partial L}\left(-\frac{\mu_1^2}{2L^2} - \mu_2 K^{(0,0)}(L,G)\right) \tag{39}$$

$$\dot{g} \equiv \frac{\partial}{\partial G}\left(-\mu_2 K^{(0,0)}(L,G)\right) . \tag{40}$$

Poincaré (1902) was the first to study motion in the vicinity of a resonance in the restricted three-body problem by means of a Hamiltonian without any perturbing terms other than the resonant ones. This Hamiltonian is also called the zero-order resonance Hamiltonian. In order to reduce the degrees of freedom of the Hamiltonian, we perform a canonical transformation to the Poincaré resonance variables,

$$\phi = l + g - t \tag{41}$$

$$\psi = (p+q)l - p(t-g) \tag{42}$$

via the generating function

$$\mathscr{F} = \{(p+q)l - p(t-g)\}\,\Psi + (l+g-t)\Phi . \tag{43}$$

Note that ψ has the same form as the resonance variable φ used previously. The respective conjugate momenta are

$$\Phi = ((p+q)G - pL)/q \tag{44}$$

$$\Psi = (L-G)/q . \tag{45}$$

In terms of the orbital elements, these can be written as

$$\Phi = \sqrt{\mu_1 a}\left\{\frac{(p+q)\sqrt{1-e^2} - p}{q}\right\} \tag{46}$$

$$\Psi = \sqrt{\mu_1 a}\left\{\frac{1-\sqrt{1-e^2}}{q}\right\} . \tag{47}$$

Hence the new Hamiltonian, $\mathscr{H}'$ can be written as

$$\mathscr{H}' = \mathscr{H} + \frac{\partial \mathscr{F}}{\partial t} = -\frac{\mu_1^2}{2(\Phi + (p+q)\Psi)^2} - p\Psi - \Phi - \mathscr{R} \tag{48}$$

where $\mathscr{R}$ is to be written in terms of the new variables. Note that $\mathscr{H}'$ is explicitly time independent and is thus a constant of the motion.

In terms of the Poincaré variables ψ is the resonant argument and the resonance condition is

$$\dot{\psi} = \frac{\partial}{\partial \Psi}\left\{\frac{-\mu_1^2}{2(\Phi+(p+q)\Psi)^2} - p\Psi - \Phi - \mu_2 K^{(0,0)}\right\} = 0 \tag{49}$$

The term $\mu_2 K^{(0,0)}$ is a secular term. Since it only serves to shift the position of the resonance by a quantity of order μ_2, it can be ignored.

The zero-order resonance Hamiltonian must contain all those terms with nearly stationary arguments, i.e., those independent of ϕ. Let

$$K_i = K^{(i(p+q),-ip)} \tag{50}$$

and set $q = 1$ to consider just interior, first-order resonances. Ignoring K_i for $i \neq 1$ (i.e. ignoring all arguments which are multiples of the resonant one), and changing $p+q$ to j_1 to be consistent with our previous notation, the zero-order resonance Hamiltonian can be written as

$$\mathscr{H}^0_{j_1 1} = \frac{-\mu_1^2}{2(\Phi + j_1\Psi)^2} - (j_1+1)\Psi - \Phi - \mu_2 K_1 \cos\psi \tag{51}$$

Since this Hamiltonian is independent of ϕ, Φ is also a constant of the motion. The contours of constant $H^0_{j_1 1}$ on surfaces of constant Φ have been studied many times (see, for example, Message 1966 and Wisdom 1980). For a given resonance there are usually two critical values of Φ which separate qualitatively different types of contours. Fig. 4 illustrates the contours of these different regions using the Cartesian coordinates $\xi = \sqrt{2\Psi}\sin\psi$ and $\eta = \sqrt{2\Psi}\cos\psi$. In this coordinate system the radial distance is directly proportional to e. The stable and unstable equilibrium points are marked by a '•' and a '○' respectively. Though all the contours are symmetric about $\xi = 0$, it is not obvious from the form of the Hamiltonian that all the equilibrium points lie on the ξ axis. That this is in fact the case for the interior region ($a < 1$) was shown by Message (1958). The regions in which ψ librates are shaded.

For $\Phi < \Phi_1$ there is only one equilibrium point for which $\psi = 0$, and only one libration region (see Fig. 4(a)). The libration and circulation regions are separated by the contour which passes through the origin. This contour crosses the η axis again at $\eta_{\max} = \sqrt{2\Psi_{\max}}$, where $\Psi_{\max}$ is defined by

$$\mathscr{H}^0_{j_1 1}(\Phi, \Psi = 0) = \mathscr{H}^0_{j_1 1}(\Phi, \Psi_{\max}, \psi = 0) . \tag{52}$$

As Φ is increased to Φ_1, a cusp appears (Fig. 4(b)) which then bifurcates into a stable and an unstable point for $\Phi > \Phi_1$. At this stage there are now two libration regions: one about $\psi = 0$ and the other about $\psi = \pi$.

The interval is further subdivided by Φ_2, which is the value of Φ when the separatrix passes through the origin. For $\Phi_1 < \Phi < \Phi_2$ the libration region about $\psi = \pi$ is defined by the separatrix while the libration region about $\psi = 0$ is defined by the contour that passes through the origin (see Fig. 4(c)).

For $\Phi_2 < \Phi < \sqrt{\mu_1}$ the libration region about $\psi = 0$ is defined by the separatrix while the libration region about $\psi = \pi$ is defined by the contour that passes through the origin (see Fig. 4(d)). Wisdom (1980) also found another bifurcation for $\Phi > \sqrt{\mu_1}$. However, these values of Φ are not relevant to the present study and will not be considered further.

A diagram of the equilibrium points in terms of η for different values of Φ is shown in Fig. 5. Note that the two distinct branches of stable equilibrium points are asymptotic to $\eta = 0$ and hence, since $\xi = 0$ at an equilibrium point, never correspond to $e = 0$.

In order to locate and measure the region of libration about $\psi = 0$ in terms of a and e for particles that start at pericentre on the line of inferior conjunction, we adopt the procedure used by Wisdom (1980). Given particular values of a_0 and e_0, the values of Φ_0 and Ψ_0 are calculated using Eqs. (46) and (47). The test

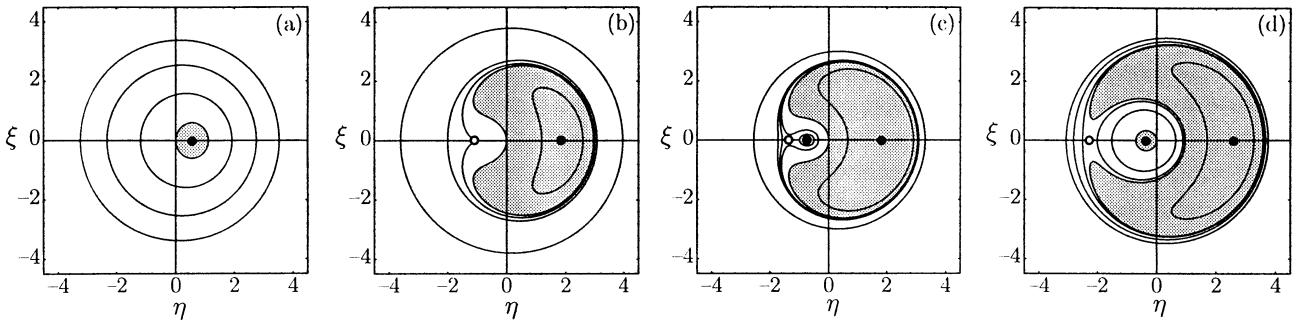

Fig. 4a–d. Contours of constant Hamiltonians plotted in terms of $\xi = \sqrt{2\Psi}\sin\psi$ and $\eta = \sqrt{2\Psi}\cos\psi$ for different ranges of Φ (see text). The stable and unstable equilibrium points are denoted by • and ○, respectively. The shaded areas show the libration regions. The relevant values of Φ are: **a** $\Phi < \Phi_1$. **b** $\Phi = \Phi_1$. **c** $\Phi_1 < \Phi < \Phi_2$. **d** $\Phi_2 < \Phi < \sqrt{\mu_1}$.

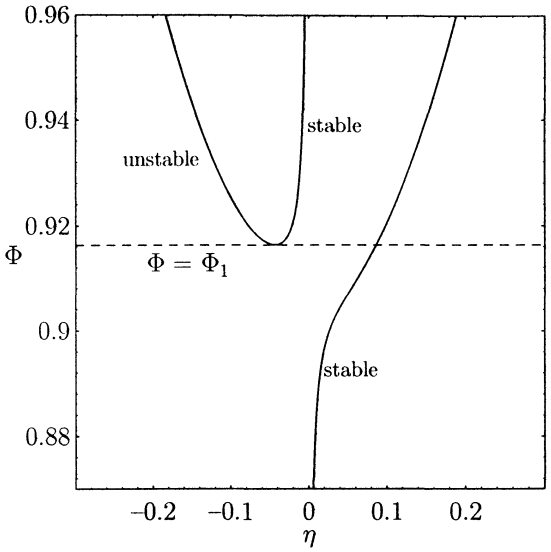

Fig. 5. Diagram of the value of η for the stable and unstable equilibrium points for the Hamiltonian given by Eq. (51) for the 4:3 resonance. The shape of the curves in this diagram is similar to that for other first-order resonances.

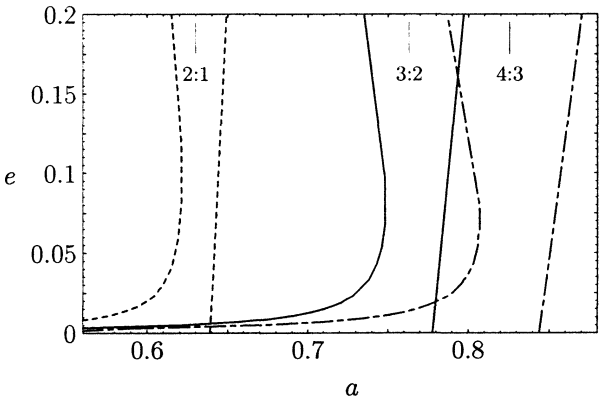

Fig. 6. Libration regions in (a, e) space using the Hamiltonian given by Eq. (51) for the 2:1, 3:2 and 4:3 resonances with libration about $\psi = 0$. The location of the nominal resonant semimajor axes are indicated at the top of the diagram.

for resonant libration about $\psi = 0$ is as follows: If $\Phi_0 < \Phi_2$, then ψ librates if $\Psi_0 < \Psi_{\max}(\Phi_0)$, where $\Psi_{\max}$ is defined by the contour which passes through the origin; if $\Phi_0 > \Phi_2$ then ψ librates if $\Psi_{\min}(\Phi_0) < \Psi_0 < \Psi_{\max}(\Phi_0)$, where $\Psi_{\min}$ and $\Psi_{\max}$ are defined by the contour that passes through the unstable equilibrium point. Fig. 6 shows the results of such computations for the 2:1, 3:2 and 4:3 resonances using $\mu_2 = 10^{-3}$.

For $e < 0.02$ the libration regions are broad and there is an overlap at most semimajor axes. At first glance this phenomenon seems to be similar to that shown in Fig. 3 (solid lines) although, in fact, each has a completely different origin. This will be discussed in more detail in Sect. 5. For analytical studies of the motion the Hamiltonian considered in Eq.(51) is usually simplified in two different ways depending on the orbital eccentricity of the particle. In the following subsections we study the two approaches.

4.1. Large eccentricity

For relatively large eccentricities ($e \geq 0.15$), the pendulum model is usually considered. This is based on the assumption that the system is close to the nominal resonant position, given by the resonance condition. Therefore, it is possible to make some approximations in the Hamiltonian (Eq. (51)). These are (i) that $K_1(\Phi, \Psi)$ is sufficiently well approximated near the resonance by $K_1(\Phi, \Psi_{\rm res})$, where $\Psi_{\rm res}$ is defined implicitly by the resonance condition, and (ii) that the first three terms of the Hamiltonian (on the right-hand side of Eq. (51)) are sufficiently well approximated by the quadratic terms in its Taylor series expansion about $\Psi = \Psi_{\rm res}$. In these circumstances Eq. (51) can be approximated as

$$\mathscr{H}^*(\Psi^*, \psi) = A_0 + A_1\Psi^* + A_2{\Psi^*}^2 + B_0\cos\psi \tag{53}$$

where

$$\Psi^* = \Psi - \Psi_{\rm res} \tag{54}$$

and A_0, A_1, A_2 and B_0 are constants given by

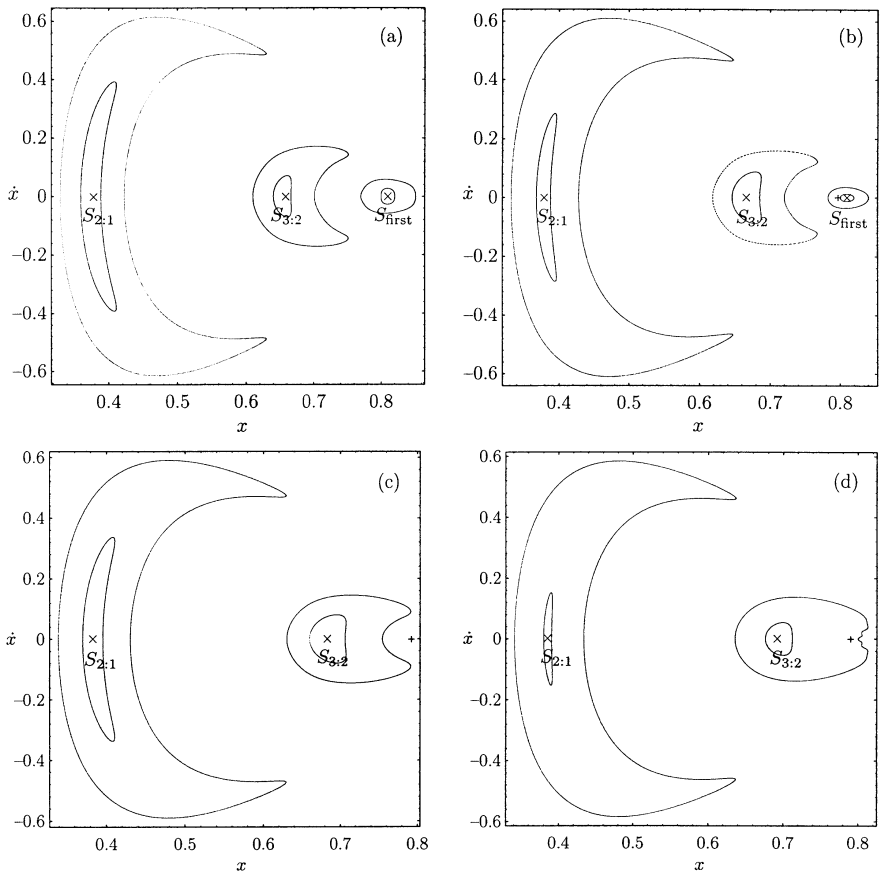

Fig. 7a–d. Poincaré surfaces of section for **a** $C_{\rm J} = 3.040$, **b** $C_{\rm J} = 3.044$, **c** $C_{\rm J} = 3.049$ and **d** $C_{\rm J} = 3.052$. The single points inside the islands, represented by $\times$ and named $S_{2:1}$, $S_{3:2}$ and $S_{\rm first}$, are used to show the location of the stable fixed points for the 2:1 and 3:2 resonances and the periodic orbit of the first kind, respectively. The location of the $e = 0$ point (i.e. zero osculating eccentricity at $t = 0$) is denoted by $+$ when it is in a location different from $S_{\rm first}$. The largest islands around each of the points are the furthest regular orbits associated with them, giving the boundary of each family of regular orbits. In the case of the resonances shown in (**a**), (**b**) and (**c**) these islands correspond to the actual maximum amplitude of libration around a pericentric position.

$$A_0 = \frac{-\mu_1^2}{2(\Phi + j_1\Psi_{\rm res})^2} - (j_1+1)\Psi_{\rm res} - \Phi$$
$$= -\frac{\mu_1}{2a_{\rm res}} - \sqrt{\mu_1 a_{\rm res}(1-e_{\rm res}^2)} \quad (55)$$

$$A_1 = \frac{j_1\mu_1^2}{(\Phi + j_1\Psi_{\rm res})^3} - (j_1+1)$$
$$= -(j_1+1) + j_1\sqrt{\frac{\mu_1}{a_{\rm res}^3}} = 0 \quad (56)$$

$$A_2 = \frac{-3j_1^2\mu_1^2}{2(\Phi + j_1\Psi_{\rm res})^4} = -\frac{3j_1^2}{2a_{\rm res}^2} = \text{const.} \quad (57)$$

$$B_0 = -\mu_2 K_1(\Psi_{\rm res}, \Phi) = -\mu_2 f(\alpha_{\rm res}) e_{\rm res} = \text{const.} \quad (58)$$

and, since we are taking $a' = 1$, we have $\alpha_{\rm res} = a_{\rm res}$. Note that $A_1 = 0$ because this is the resonance condition. The level curves of this Hamiltonian are then explicitly

$$\Psi = \Psi_{\rm res} \pm \left\{ \frac{\mathscr{H}^* - A_0 - B_0\cos\psi}{A_2} \right\}^{1/2} . \quad (59)$$

The contours that form the boundary of the libration region, the separatrices, are given by

$$\Psi_{\rm sep} = \Psi_{\rm res} \pm \Delta\Psi \cos\frac{\psi}{2} \quad (60)$$

where the resonance half-width, $\Delta\Psi$, is defined by $\Delta\Psi = (2B_0/A_2)^{1/2}$. This result is similar to that obtained for the pendulum approach in Sect. 3 and hence a plot of the phase space would be similar to that given in Fig. 2 and an a–e plot of the maximum libration would be similar to the dashed line plots given in Fig. 3.

4.2. Small eccentricity

For small eccentricities, $e \leq 0.15$, the *second fundamental model of resonance* (Henrard & Lemaître 1983) is commonly adopted; Hamiltonians of this kind were first used by Andoyer (1903). The second fundamental model of resonance is based on the assumption that the eccentricity of the particle's orbit is small, no matter how far the system is from the nominal resonant position. In this case the momenta can be approximated by

$$\Psi = \sqrt{\mu_1 a}\, e^2/2 \quad (61)$$
$$\Phi = \sqrt{\mu_1 a}\,(1 + j_1 e^2/2)\,. \quad (62)$$

Therefore, expanding the two-body contribution of the resonance Hamiltonian, Eq. (51), about $\Psi = 0$, since e is small, and retaining only the quadratic terms one gets Andoyer's Hamiltonian

$$\mathscr{H}^\dagger = D_0 + D_1\Psi + D_2\Psi^2 - \mu_2\sqrt{\frac{2\Psi}{\Phi}} f(\alpha_\Psi)\cos\psi \quad (63)$$

where

$$D_0 = -\left(\frac{\mu_1^2}{2\Phi^2} + \Phi\right) \tag{64}$$

$$D_1 = \left(-\frac{j_1\mu_1^2}{\Phi^3} + (j_1+1)\right) \tag{65}$$

$$D_2 = \left(-\frac{3j_1^2\mu_1^2}{2\Phi^4}\right) \tag{66}$$

and

$$\alpha_\Psi = \alpha(\Phi, \Psi = 0) = \frac{\Phi^2}{\mu_1 a_2} \ . \tag{67}$$

Qualitatively this approach produces the same results as those obtained from the original Hamiltonian given by Eq. (51). This is to be expected since the latter was derived by considering just the terms of the disturbing function up to first order in e. Therefore, at least qualitatively, $\mathscr{H}^\dagger$, produces the same behaviour as shown in Figs. 4, 6.

5. Numerical results

In this section we present an analysis of first-order resonances in the interior region using data derived from Poincaré surfaces of section. The existence of the Jacobi constant in the circular restricted three-body problem means that we can represent the trajectory in the four-dimensional phase space using just the values of x and $\dot{x}$ when $y = 0$ and $\dot{y} > 0$. The procedure is described in more detail in Hénon (1966) and Winter & Murray (1994a).

Using Poincaré surfaces of section we can follow the evolution of the islands of stability associated with the 2:1, 3:2 and 4:3 resonances as the value of the Jacobi constant changes. Our main goal is to compare our results for the libration regions associated with these first-order resonances with the widths predicted from the analytical theories presented above.

Fig. 7 and Fig. 8 show representative Poincaré surfaces of section illustrating the evolution of the libration regions associated with the interior 2:1 and 3:2 resonances as the value of the Jacobi constant increases. In these plots we have removed all points that are not relevant to our study.

In Fig. 7(a) the single points inside the islands, represented by '$\times$' and named $S_{2:1}$, $S_{3:2}$ and $S_{\rm first}$, are used to show the location of the stable fixed points for the 2:1 and 3:2 resonances and the periodic orbit of the first kind ($e = 0$), respectively. The location corresponding to $e = 0$ divides the points on the x-axis into pericentric positions (at smaller x) and apocentric ones (at larger x). The largest islands around each of the points are the furthest regular orbits associated with each resonance or periodic orbit, giving the boundary of each family of regular orbits. In the case of the resonances they correspond to the actual maximum amplitude of libration around a pericentric position. At this stage the three families of regular orbits are widely separated and do not affect one another. As the value of the Jacobi constant increases the $S_{2:1}$ and $S_{3:2}$ points move to a larger value of x and towards the location corresponding to $e = 0$. At the same time the $S_{\rm first}$ fixed point moves to a lower value of x at the location for $e = 0$ and starts to feel the influence of another stable fixed point.

For a larger value of the Jacobi constant (see Fig. 7(b)) $S_{3:2}$ gets close enough to $S_{\rm first}$ such that $S_{\rm first}$ moves to a location different from $e = 0$ (denoted by $+$). From the topological point of view nothing has changed, but there is a physical consequence: there are orbits in the family of regular orbits of $S_{\rm first}$ in which the resonant argument associated with the 3:2 resonance is librating about the apocentre. In fact $S_{\rm first}$ is the centre of this libration. Note that $S_{\rm first}$ is still relatively far from the 3:2 resonance.

As the Jacobi constant increases the family of regular orbits associated with $S_{\rm first}$ shrinks until it is completely destroyed (see Fig. 7(c)). As this evolution continues the point corresponding to $e = 0$ eventually moves inside the $S_{3:2}$ family of regular orbits (see Fig. 7(d)). The physical consequence is that the family of orbits that are librating in the 3:2 resonance is a subset of the family of regular orbits of $S_{3:2}$.

The continuation of this process is illustrated in Fig. 8. For the value of the Jacobi constant used in Fig. 8(a) $S_{3:2}$ reaches $e = 0$ and the 3:2 resonance disappears completely becoming $S_{\rm first}$.

At a larger value of the Jacobi constant, the influence of the 2:1 resonance on $S_{\rm first}$ is clear (see Fig. 8(b)). $S_{\rm first}$ has moved away from the $e = 0$ point generating an apocentric libration family for the 2:1 resonance. As $C_{\rm J}$ increases the maximum libration of this family also increases and the location of the $e = 0$ point enters the region of the $S_{2:1}$ regular orbits reducing the size of the pericentric libration family (see Fig. 8(c)). Comparison of Fig. 8(b) and Fig. 8(c) shows that the family of regular orbits of $S_{\rm first}$, itself enveloped by the family of regular orbits $S_{2:1}$, is shrinking. This family ends as the stable fixed point ($S_{\rm first}$) and the unstable fixed point of the system coalesce.

In Fig. 8(d) the family of $S_{\rm first}$ has just disappeared and the evolution of the libration family of the resonance 2:1 is in its final stages. In fact this family continues to get smaller until it disappears when $S_{2:1}$ reaches the $e = 0$ point at $C_{\rm J} = 3.222$.

A clear difference between the evolution of the 2:1 and 3:2 resonances is that in the case of the 3:2 resonance the family of regular orbits with centre at an apocentre position, $S_{\rm first}$, is destroyed in its very early stages with the orbits becoming chaotic, while for the 2:1 case it persists until its 'natural end' when the unstable and the stable fixed points coalesce and disappear. Comparing the sequence in Figs. 8(b,c,d) with the sequence in Figs. 4(d,c,b) generated by the second fundamental model of resonance, we see that the analytical model is a good predictor of the topology of the phase space for low e.

A diagram showing the relationship between the x value of the location of the $S_{2:1}$, $S_{3:2}$, $S_{4:3}$ and $S_{\rm first}$ stable points as a function of the Jacobi constant, $C_{\rm J}$, was constructed from the Poincaré surfaces of section for $2.94 < C_{\rm J} < 3.26$ (see Fig. 9). Fig. 9(a) gives the global picture for the 2:1, 3:2 and 4:3 resonances while Fig. 9(b) is an enlargement of part of Fig. 9(a) showing the details for the 4:3 resonance. The dashed line corresponds to the location of the $e = 0$ point. The full lines below this dashed line denote the location of the stable points for peri-

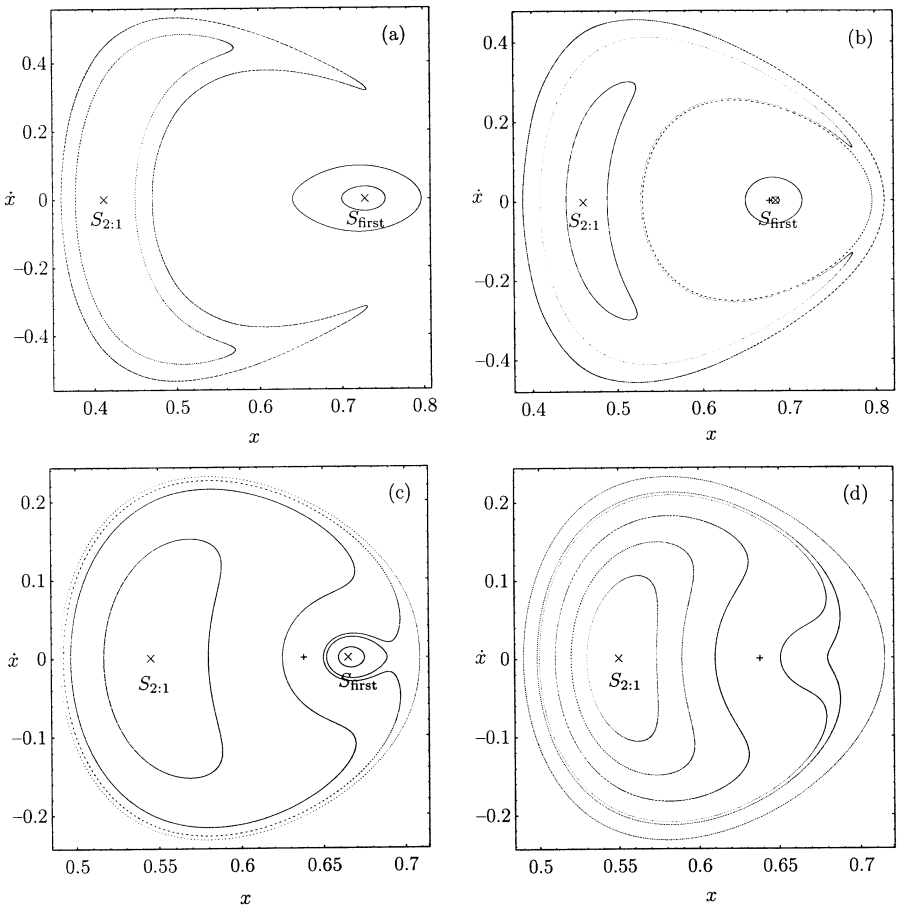

Fig. 8a–d. Poincaré surfaces of section for **a** $C_J = 3.079$, **b** $C_J = 3.120$, **c** $C_J = 3.163$ and **d** $C_J = 3.165$. The annotation is the same as in Fig. 7. In the case of the 2:1 resonance in (**a**) the curve corresponds to the actual maximum amplitude of libration around a pericentric position. Note the change in scale between **a** and **b**, and **c** and **d**.

centric libration at the 2:1, 3:2 and 4:3 resonances. The full lines above the dashed line denote the location of the stable points for apocentric libration at the 2:1 and 3:2 resonances.

Fig. 9 shows three different kinds of evolution of the stable equilibrium points associated with first-order resonances. First, the 2:1 pericentric libration curve seems to go asymptotically to the dashed line, although it is possible it could intersect it for large values of C_J. Second, the 3:2 pericentric curve has a smooth transition to the 2:1 apocentric libration curve. This means that as the value of C_J increases the centre of the 3:2 pericentric resonance moves to a smaller eccentricity, becomes a periodic orbit of the first kind at the $e = 0$ point, and then evolves to become the centre of the 2:1 apocentric resonance. At first glance this type of evolution seems to be valid for all first-order resonances of the form $p + 1 : p$ with $p \geq 2$. However, there is another factor which can affect this smooth transition. Wisdom (1980) demonstrated that the mass ratio determines the extent of the overlap of adjacent first-order resonances. Significant overlap can eliminate stable regions associated with all first-order resonances above a critical value of p (Wisdom 1980). For the mass ratio used in this study ($\bar{m}_2 = 10^{-3}$) part of the stable region associated with the 4:3 resonance (a region of small eccentricity) is destroyed and becomes a chaotic region. Therefore, the third kind of evolution shown in Fig. 9 is the one where the 4:3 pericentric libration curve ends abruptly before it reaches the dashed line (see Fig. 9(b)).

Fig. 6 of Winter & Murray (1994a) shows that the $e = 0$ point only occurs in the phase space for $C_J > 3.027$. Our full numerical integrations show that the family of periodic orbits of the first kind appears only for $C_J > 3.039$, while the 4:3 resonance disappears at $C_J > 3.037$ (see Fig. 9(b)). Since these two families of periodic orbits do not co-exist they cannot interact to produce a family of orbits in apocentric libration. Therefore in reality no apocentric libration occurs for the 4:3 resonance, or indeed for any $p + 1 : p$ first-order resonance with $p \geq 3$.

The actual regions of maximum amplitudes of libration can be obtained from the Poincaré surfaces of section when the particle is at the line of conjunction at pericentre (or apocentre in the case of apocentric libration). In Fig. 10 we show the regions of maximum amplitude of libration in (a, e) space for the 2:1, 3:2 and 4:3 resonances librating about $\psi = 0$ (full lines) and for the 2:1 resonance librating about $\psi = \pi$ (dashed line). From this diagram we have a clear picture of the actual extent of the libration at each resonance.

Fig. 10 also shows the connection between the regions associated with libration in the 2:1 resonance about $\psi = \pi$ and those associated with libration in the 3:2 resonance about $\psi = 0$. A comparison of this result for $e \geq 0.15$ with the pendulum model (Fig. 3) reveals the shortcomings of the pendulum model. In the full integrations, for low e, the shift in the location of the centre of the resonance is large. The shift is to the left (smaller a) for $\psi = 0$ and to the right (large a) for $\psi = \pi$, as expected from our

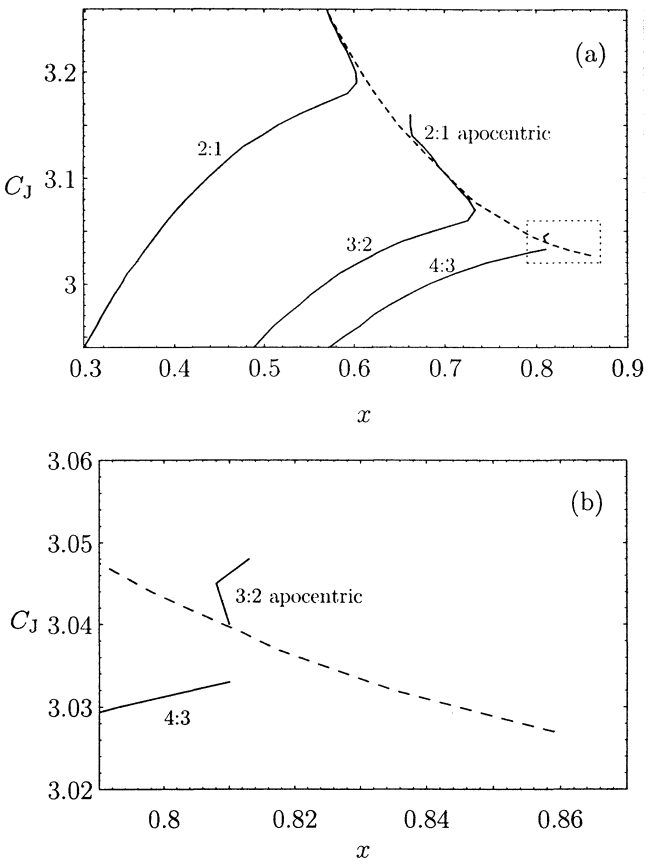

Fig. 9a and b. The relationship between the x value of the location of the stable equilibrium points and the Jacobi constant, C_J, determined by Poincaré surfaces of section obtained from numerical integrations of the full equations of motion. The dashed line corresponds to the location of the $e = 0$ points. Solid curves below this dashed line are for the centres of pericentric libration. Solid curves above this dashed line are for the centres of apocentric libration. **a** Global picture of the evolution. **b** Enlargement of the region containing the 4:3 resonance.

analysis in Sect. 3. Comparing the pericentric libration in the lower part ($e \leq 0.2$) of Fig. 10 with Fig. 6 generated from Andoyer's Hamiltonian, it is clear that there is broad agreement; the right-hand sides of the libration areas are almost vertical straight lines, and the left-hand sides show a broadening for moderate e and a narrowing for lower e. However, for $e \leq 0.02$ there is an obvious disagreement— the full integrations show there is no overlap of the libration regions of the 2:1, 3:2 and 4:3 resonances. If there was overlap such a region would be chaotic whereas our results show that the region is regular, and is mainly divided into libration in the 3:2 resonance or libration in the 2:1 resonance. Furthermore, from the Poincaré surfaces of section (see chap. 3 of Winter 1994, or in more detail, Winter & Murray 1994a) we know that particles in the region between the two resonances mostly move in regular orbits associated with circulation or libration in higher order resonances.

The overlap of the libration regions of first-order resonances for very small eccentricities (shown by the solid curves in Fig. 3 and in Fig. 6) were obtained using two different approachs and have different origins despite their similarities. In our full numerical integration using Poincaré surfaces of section this feature does not appear. The reason why this feature appeared in the pendulum approach used by Dermott & Murray (1983) is that the borders of the libration region were defined in terms of the separatrix that passes through the unstable equilibrium point. For very low eccentricities we have seen that the system has no unstable equilibrium point; this means that there is no separatrix and consequently it does not make sense to define the libration region in terms of the separatrix. The division between libration and circulation has to be defined in terms of the trajectory that has the $e = 0$ point as we did in Sect. 4 (after Wisdom 1980). In the case of the approach using the second fundamental model of resonance, the cause of the overlap is that the centre of the resonance never reaches the $e = 0$ point. The diagram of stable equilibrium points determined from our numerical results (Fig. 9) shows that in the case of the 2:1 resonance, the $e = 0$ point may never be reached. However, the same diagram shows that the centre of the 3:2 resonance will always reach the $e = 0$ point.

In their paper on the structure of the Kirkwood gaps in the asteroid belt, Dermott & Murray (1983) showed a plot similar to Fig. 3 together with the location of the asteroids in (a, e) space. They showed that there was a good correspondence between the maximum width of the resonances and the width of the observed gaps. They also pointed out that the value of $|a'\mathscr{R}/\mathscr{G}m'|$ for a given first-order resonance increases as the semimajor axis of the resonance approaches that of Jupiter. Since the width of a resonance is proportional to the square root of $|\mathscr{R}|$, and hence the square root of the constant in the pendulum-like equation ($\mathscr{C}$ in our notation), they expected the resonance width to increase as a increases. Similarly, the second fundamental model of resonance predicts a widening of the first-order resonances as $\alpha \rightarrow 1$ (see Fig. 6). The results of our measurements (see Fig. 10) show the opposite result. When the full problem is integrated it is clear that the actual resonance width decreases as a increases. This can be partly understood if we plot the predictions shown in Fig. 3 with the actual measurements (see Fig. 10 and the solid lines in Fig. 11). This shows that at the 2:1 resonance, apart from the behaviour at very low e, the agreement is excellent. This is because the 2:1 resonance is relatively isolated from the next two first-order resonances; this is also clear from the surfaces of section shown in Figs. 7 and 8. For the 3:2 and 4:3 resonances there is little agreement between the observed and calculated widths; this might have been expected from the extent of the predicted overlap (see Fig. 3 and the dotted lines in Fig. 11) and the resulting increase in the extent of the chaotic regions (see Winter & Murray 1994a for further evidence of this phenomenon). Here the effect of these first-order resonances on each other is considerable. Although the inner edge of the 3:2 resonance at moderate e is reasonably well approximated by the second fundamental model, its outer edge and the boundary of the 4:3 resonance are not.

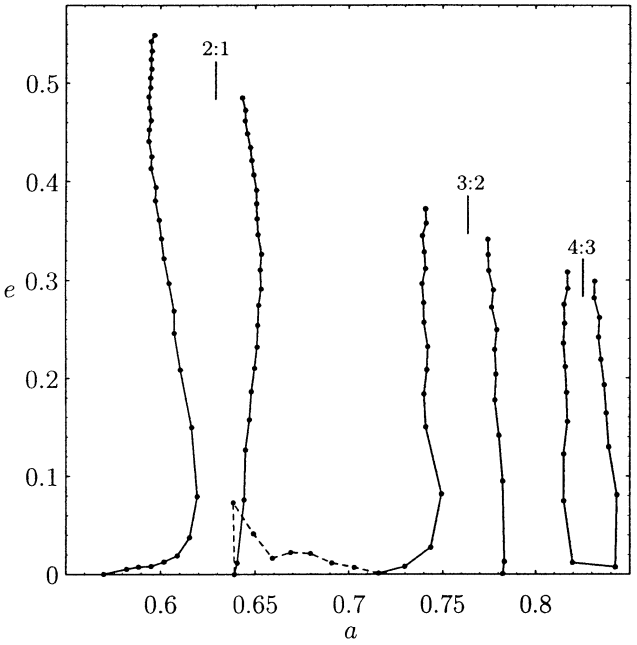

Fig. 10. Libration regions in the *a–e* space obtained from the Poincaré surfaces of section. The full lines are for the 2:1, 3:2 and 4:3 resonances librating about $\psi = 0$ and the dashed line is for the 2:1 resonance librating about $\psi = \pi$. Note that the libration region associated with the 4:3 resonance does not reach the $e = 0$ curve since it becomes chaotic (see Fig. 9(b)).

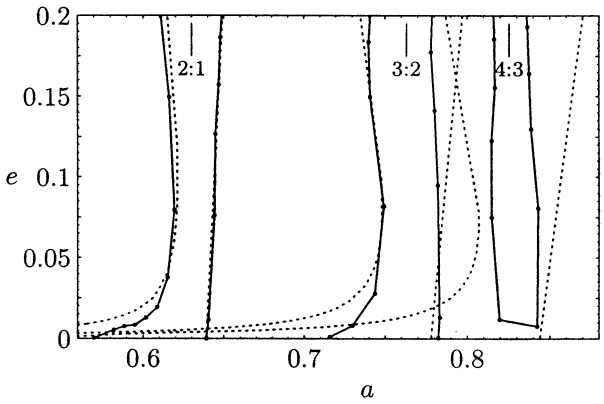

Fig. 11. Predicted maximum libration regions in *a–e* space from Fig. 6 (dotted lines) and those obtained from the Poincaré surfaces of section in Fig. 10 (solid lines). The nominal semimajor axes of the 2:1, 3:2 and 4:3 resonances are indicated.

6. The 2:1 resonance

In this section we show the time evolution of the orbital elements and other parameters for a sample of trajectories in the vicinity of the 2:1 resonance. This serves to classify and illustrate the various types of regular behaviour that are possible at first-order resonances. In each of the following diagrams we show (a) the evolution of the semimajor axis a, eccentricity, e, longitude of the pericentre, ϖ, and the resonant argument, $\varphi = 2\lambda' - \lambda - \varpi$, (b) the corresponding Poincaré surfaces of section in x and $\dot{x}$, and (c) the quantities $\xi = \sqrt{2\Psi}\sin\psi$ and $\eta = \sqrt{2\Psi}\cos\psi$ used in Sect. 4. Recall that the radial distance from the origin in a (η, ξ) plot is a linear function of the eccentricity. Note also that while the $(x, \dot{x})$ plots are surfaces of section, the (η, ξ) plots simply show the evolution of ξ and η. The nominal resonant semimajor axis for the 2:1 resonance is $a \approx 0.629$ and this is indicated by the dashed line in the evolution of a in each plot. In each plot the limits of a, e, ϖ and φ are 0.6 to 0.65, 0 to 0.25, $-\pi$ to π and $-\pi$ to π respectively. Note that for the purposes of comparison, the scales are the same in the corresponding parts of Figs. 12–17

Fig. 12 shows the orbital evolution of a particle in *almost exact pericentric resonance*, with initial conditions $C_J = 3.163$, $x = 0.545$ and $y = \dot{x} = 0$; this corresponds to $a = 0.625$, $e = 0.128$, $\varpi = 0$ and $\lambda = 0$. The resulting trajectory is very close to the centre of the 2:1 resonance with $\varphi = 0$, as indicated by $S_{2:1}$ in Fig. 8(c). Note that φ is almost constant ($\varphi \approx 0$), a and e have very small amplitudes of oscillation and ϖ circulates with a relatively large period.

The results of the evolution for a trajectory librating about the 2:1 resonance with *large amplitude of libration* are shown in Fig. 13. The initial conditions for this trajectory are $C_J = 3.163$, $x = 0.63$ and $y = \dot{x} = 0$; this corresponds to $a = 0.638$, $e = 0.012$, $\varpi = 0$ and $\lambda = 0$. This trajectory corresponds to the one with the largest amplitude of libration about the 2:1 resonance shown in Fig. 8(c). The amplitude of libration of φ about pericentre is almost 2π and hence a and e also show a large amplitude of oscillation with $0.012 \leq e \leq 0.2$. On the other hand ϖ oscillates with a small amplitude since e is relatively large, as discussed in Sect. 3. Also note that after about $t = 40$, ϖ changes more rapidly as e approaches its minimum value.

The case of a trajectory in the *low eccentricity libration* at the 2:1 resonance is shown in Fig. 14. The particle has initial conditions $C_J = 3.210$, $x = 0.5995$ and $y = \dot{x} = 0$; this corresponds to $a = 0.602$, $e = 0.004$, $\varpi = 0$ and $\lambda = 0$. This trajectory is close to a periodic orbit of the first kind. However, note that φ has a small amplitude of libration about 0, and consequentely, a and e also have small amplitudes. Since e remains very small, ϖ circulates quickly, with $\dot{\varpi} < 0$. Thus the resonant a is much smaller than the nominal value, as expected from our analysis in Sect. 3. Note also that the trajectory in the ξ-η plot is to the right of the origin.

Fig. 15 shows the result for a particle in *apocentric libration*, with initial conditions $C_J = 3.163$, $x = 0.675$ and $y = \dot{x} = 0$; this corresponds to $a = 0.637$, $e = 0.060$, $\varpi = \pi$ and $\lambda = 0$. This trajectory is very close to the centre of the 2:1 resonance for $\varphi = \pi$ as shown in Fig 8(c). Note that φ is almost constant ($\varphi \approx \pi$), a and e have small amplitudes of oscillation, and ϖ circulates with a relatively short period. Because $\dot{\varpi} > 0$, a is larger than the nominal value, as discussed in Sect. 3.

The results of the evolution for a trajectory in *outer circulation* about the 2:1 resonance are given in Fig. 16. The initial conditions for this trajectory are $C_J = 3.163$, $x = 0.49$ and $y = \dot{x} = 0$; this corresponds to $a = 0.611$, $e = 0.198$, $\varpi = 0$ and $\lambda = 0$. This is the largest curve shown in Fig. 8(c). In this

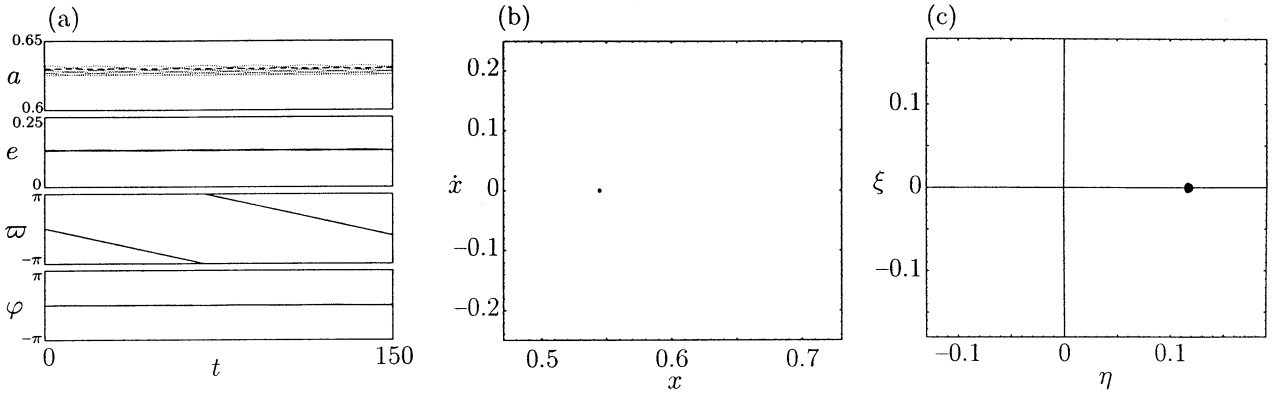

Fig. 12. a Variation of orbital elements, **b** the surface of section and **c** the ξ and η plot illustrating almost exact pericentric resonance at the 2:1 resonant location.

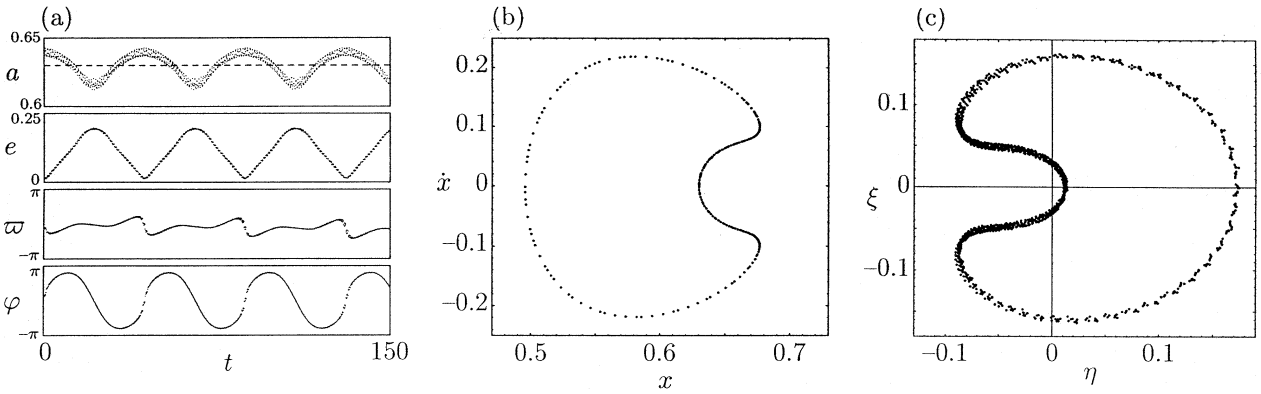

Fig. 13. a Variation of orbital elements, **b** the surface of section and **c** the ξ and η plot illustrating large amplitude libration at the 2:1 resonance.

case the resonant angle, φ, circulates relatively fast. As this is a regular trajectory the semimajor axis and eccentricity show a regular behaviour. Their amplitudes of oscillation are not very large and the longitude of the pericentre circulates with a relatively large period.

Fig. 17 shows the results for a trajectory displaying *inner circulation* (or *paradoxical circulation*) about the 2:1 resonance. The initial conditions for this trajectory are $C_J = 3.163$, $x = 0.65$ and $y = \dot{x} = 0$; this corresponds to $a = 0.638$, $e = 0.018$, $\varpi = \pi$ and $\lambda = 0$. This is the second largest curve shown in Fig. 8(c). In this case the resonant angle, φ, circulates with a much larger period than in the previous case of circulation shown in Fig. 16. Some of the intricate features of the orbital element plots can be better understood by comparing them with the Poincaré surface of section shown in Fig. 17(b). We can divide the evolution of this trajectory into two parts. In the first the particle is moving on a small curve around the stable point with $\varphi = \pi$; in the second it is moving in a large curve around the stable point with $\varphi = 0$. In the first case it gives the appearence of being an apocentric librator and in the second it gives the appearence of being in outer circulation. These two different kinds of behaviours are shown in the time evolution of φ, a, e, and even ϖ. Between about $t = 40$ and $t = 100$ orbital periods φ gives the impression of slowly librating about π, but before and after this time interval ψ circulates rapidly.

7. Conclusions

In this paper we have attempted to compare the predictions of known analytical models of resonance in the circular restricted problem with the results of numerical integrations of the full equations of motion. The numerical aspect of this work consisted of an enormous computational task, part of which has already generated two atlases of Poincaré surfaces of section (Winter & Murray, 1994a,b) giving a representative and detailed picture of large part of the phase space of the planar, circular, restricted three-body problem for a specific mass ratio. Below we highlight some important conclusions of this work.

– The technique of the Poincaré surface of section is an excellent tool for determining the nature of a trajectory and also its excursions through the phase space; it is ideally suited to the planar, circular, restricted three-body problem since this is a two-degree of freedom system with an integral of the motion.
– Both the pendulum model and the second fundamental model of resonance predict the overlap of adjacent libration regions at low eccentricity for first-order resonances (see

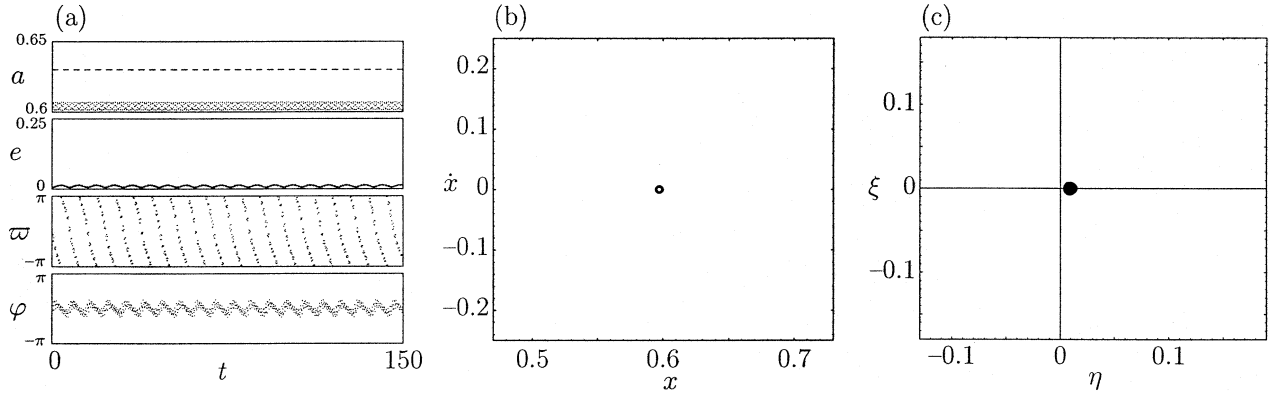

Fig. 14. a Variation of orbital elements, **b** the surface of section and **c** the ξ and η plot illustrating low eccentricity libration at the 2:1 resonance.

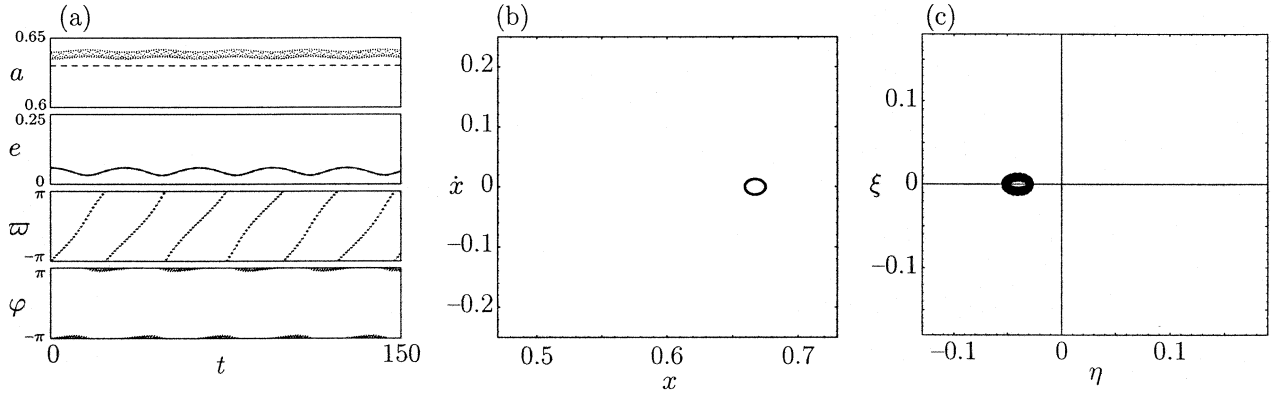

Fig. 15. a Variation of orbital elements, **b** the surface of section and **c** the ξ and η plot illustrating apocentric libration at the 2:1 resonance.

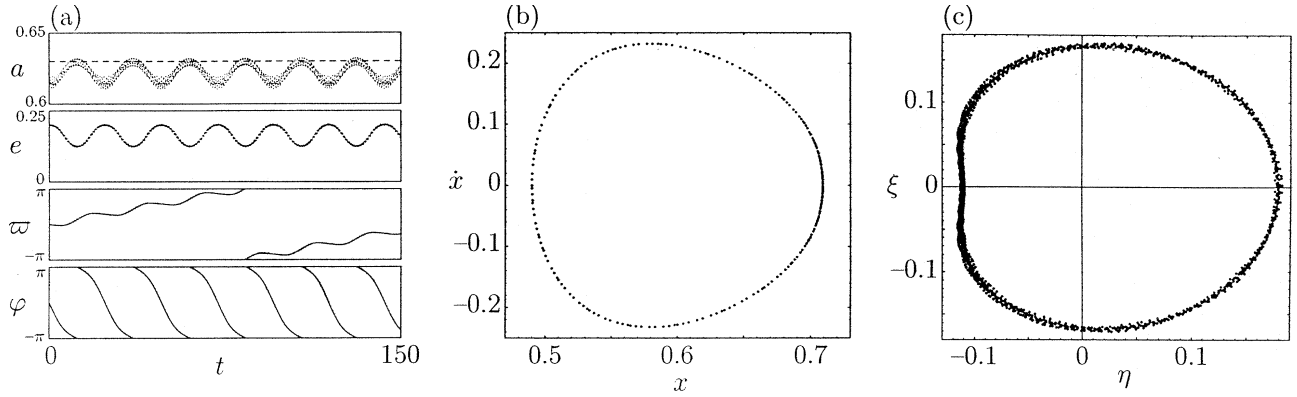

Fig. 16. a Variation of orbital elements, **b** the surface of section and **c** the ξ and η plot illustrating outer circulation at the 2:1 resonance.

Sec. 3 and 4). This leads to the incorrect conclusion that for low eccentricities the phase space should be chaotic. However, our numerical results clearly demonstrate that, for the mass ratio considered, the region of the phase space between 2:1 and 3:2 resonances, with $\varpi = 0$, is almost completely dominated by regular motion.

– We have shown that the centre of the 3:2 pericentric resonance passes through the $e = 0$ point and then becomes the centre of the 2:1 apocentric resonance. This result was only obtained because we considered the full problem which includes the interaction between the resonances. Our study of the evolution of the centre of the 4:3 pericentric resonance leads us to believe that this kind of evolution might be a general rule for all $p + 1 : p$ resonances with $p \geq 2$, provided that they have not already been destroyed by overlap with other resonances.

– Since we considered the full problem, it was possible to find the actual shape and location of the maximum amplitude of libration for the interior first-order resonances and so verify the quality of the analytical models currently used. This

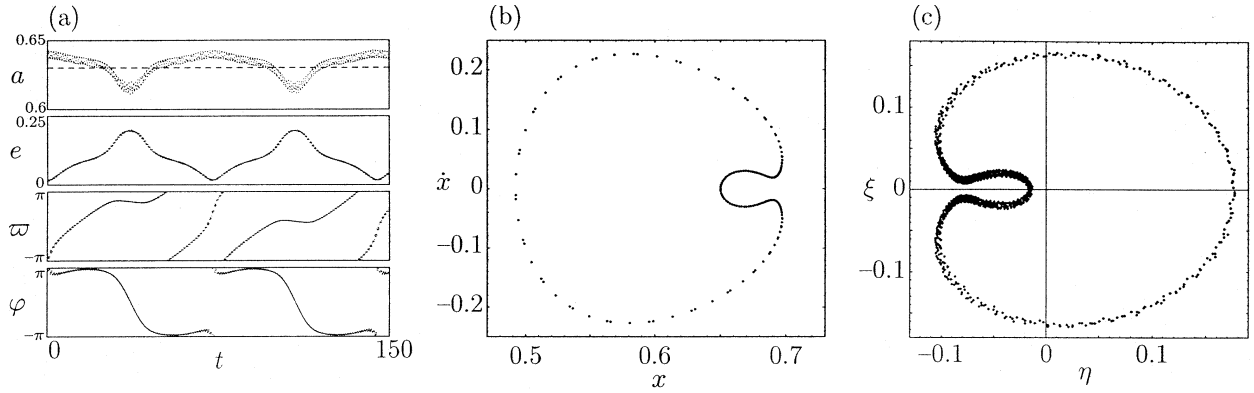

Fig. 17. a Variation of orbital elements, **b** the surface of section and **c** the ξ and η plot illustrating inner circulation at the 2:1 resonance.

shows that although the strength of the $p+1:p$ resonances increases as p increases (i.e. as the orbit of the perturber is approached), the corresponding widths of these resonances decreases due to perturbations from adjacent resonances and the resulting increase in the size of the chaotic zones associated with the separatrices.

Acknowledgements. Part of this work was funded by the UK PPARC, CAPES (proc. 445/90-1) and CNPq (proc. 520044/95-9).

References

Andoyer M. H., 1903, Bull. Astron. 20, 321

Brouwer D., Clemence G. M., 1961, Methods of Celestial Mechanics, Academic Press, New York

Chirikov B. V., 1979, Phys. Rep. 52, 263

Dermott S. F., Murray C. D., 1983, Nat 319, 201

Hénon M., 1966, Bull. Astron. 1, 57

Henrard J., Lemaître A., 1983, Celest. Mech. 30, 197

Message P. J., 1958, AJ 63, 443

Message P. J., 1966, in: The Theory of Orbits in the Solar System and in Stellar Systems, ed. G. Contopoulos, Academic Press, New York, p. 197

Murray C. D., Harper D., 1993, Expansion of the Planetary Disturbing Function to Eighth Order in the Individual Orbital Elements, QMW Maths Notes, London

Poincaré H., 1902, Bull. Astron. 19, 289

Roy A. E., Ovenden M. W., 1954, MNRAS 114, 232

Winter O. C., 1994, The Phase Space of the Planar, Circular Restricted Three-Body Problem, Dissertation, Univ. London

Winter O. C., Murray C. D., 1994a, Atlas of the Planar, Circular, Restricted Three-Body Problem. I. Internal Orbits, QMW Maths Notes, London

Winter O. C., Murray C. D., 1994b, Atlas of the Planar, Circular, Restricted Three-Body Problem. II. External Orbits, QMW Maths Notes, London

Winter O. C., Murray C. D., 1995, in: From Newton to Chaos, eds. A.E. Roy & B.A. Steves, Plenum Press, New York

Winter O. C., Murray C. D., 1996a, in: Chaos in Gravitational N-Body Systems, eds. J. Muzzio & S. Ferraz-Mello, Kluwer, Dordrecht (in press)

Winter O. C., Murray C. D., 1996b, (in preparation)

Wisdom J., 1980, AJ 85, 1122

This article was processed by the author using Springer-Verlag TEX A&A macro package version 4.